PERGAMON

Journal of South American Earth Sciences 12 (1999) 349–366

Journal of
South American
Earth Sciences

Gold in the Neoproterozoic juvenile Bossoroca Volcanic Arc of southernmost Brazil: isotopic constraints on timing and sources

M.V.D. Remus[a,*], N.J. McNaughton[b], L.A. Hartmann[a], J.C. Koppe[a], I.R. Fletcher[b], D.I. Groves[b], V.M. Pinto[a]

[a]*Instituto de Geociências, Universidade Federal do Rio Grande do Sul, Av. Bento Gonçalves 9500, 91501-970, Porto Alegre, RS, Brazil*
[b]*Centre for Strategic Mineral Deposits, University of Western Australia, Nedlands, WA 6907, Australia*

Abstract

The Neoproterozoic Bossoroca juvenile Volcanic Arc of southernmost Brazil contains arc-related gold deposits. The Bossoroca gold deposit consists of veins and stockworks of quartz-gold ores with minor pyrite, chalcopyrite, galena and tellurides. Carbonate, chlorite, sericite and tourmaline are the main gangue minerals. The ore shoots are contained in calc-alkaline pyroclastic andesites and dacites with minor basalts and epiclastic rocks of the Campestre Formation. SHRIMP U/Pb investigations of zircon show that the island-arc volcanogenic sequence was formed *ca* 757 m.y. ago in the early Brasiliano Cycle and metamorphosed into transitional greenschist/amphibolite facies of low-pressure regional metamorphism at *ca* 700 Ma. Nearby, the post-tectonic São Sepé Granite was intruded into the volcanic arc at *ca* 550 Ma. The mineralising fluids have been related either to metamorphism or to solutions derived from post-tectonic intrusive granites. Lead isotopic analyses, carried out on galena from the gold ore, on feldspar and total rock from the associated volcanic pile, and also on feldspar and total rock from the São Sepé Granite, indicate that gold mineralisation is related to the volcanogenic rocks, and that the deposit should be considered to be of an epizonal orogenic type.

Resumen

O Arco Vulcânico Juvenil da Bossoroca de idade Neoproterozóica possui depósitos de ouro relacionados a arco. O depósito de ouro da Bossoroca consiste de veios e "stock-works" de quartzo com pirita, calcopirita, galena e teluretos subordinados. Os principais minerais da ganga são carbonato, clorita, sericita e turmalina. Os filões de minério estão encaixados numa sequéncia piroclástica dacítica a andesítica calcico-alcalina com basaltos e rochas epiclásticas subordinadas. Investigações em zircões pelo método U/Pb via SHRIMP mostram que a sequência vulcanogênica do arco de ilhas foi gerada há 757 Ma durante o início do Ciclo Brasiliano e metamorfisada na transição do fácies xisto verde/anfibolito do metamorfismo regional de baixa pressão há cerca de 700 Ma. O Granito São Sepé, pós-tectônico, intrudiu no arco há cerca de 550 Ma. Os fluidos mineralizadores têm sido relacionados ao metamorfismo ou a soluções derivadas dos granitos intrusivos pós-tectônicos. Análises isotópicas de Pb de galenas provenientes do minério aurífero, de feldspatos e rocha total da sequência vulcânica associada e também em feldspatos e rocha total do Granito São Sepé indicam que a mineralização aurífera está relacionada às rochas vulcanogênicas e que o depósito de ouro deve ser considerado como do tipo epizonal orogênico.

1. Introduction

Several small, epigenetic, quartz lode-gold deposits occur in the Neoproterozoic juvenile volcanic arc in the Precambrian shield of Rio Grande do Sul State in southernmost Brazil (Koppe, 1990; Babinski et al., 1996). The majority are enclosed in Precambrian meta-volcanosedimentary sequences of low- to medium-metamorphic grade of the Vacacaí Group. Others are associated with granites and volcanic rocks formed at the end of the Precambrian to Early Paleozoic. The

* Corresponding author. Fax: +55-51-319-1811.
E-mail address: mremus@if.ufrgs.br (M.V.D. Remus).

0895-9811/99/$ - see front matter
PII: S0895-9811(99)00026-7

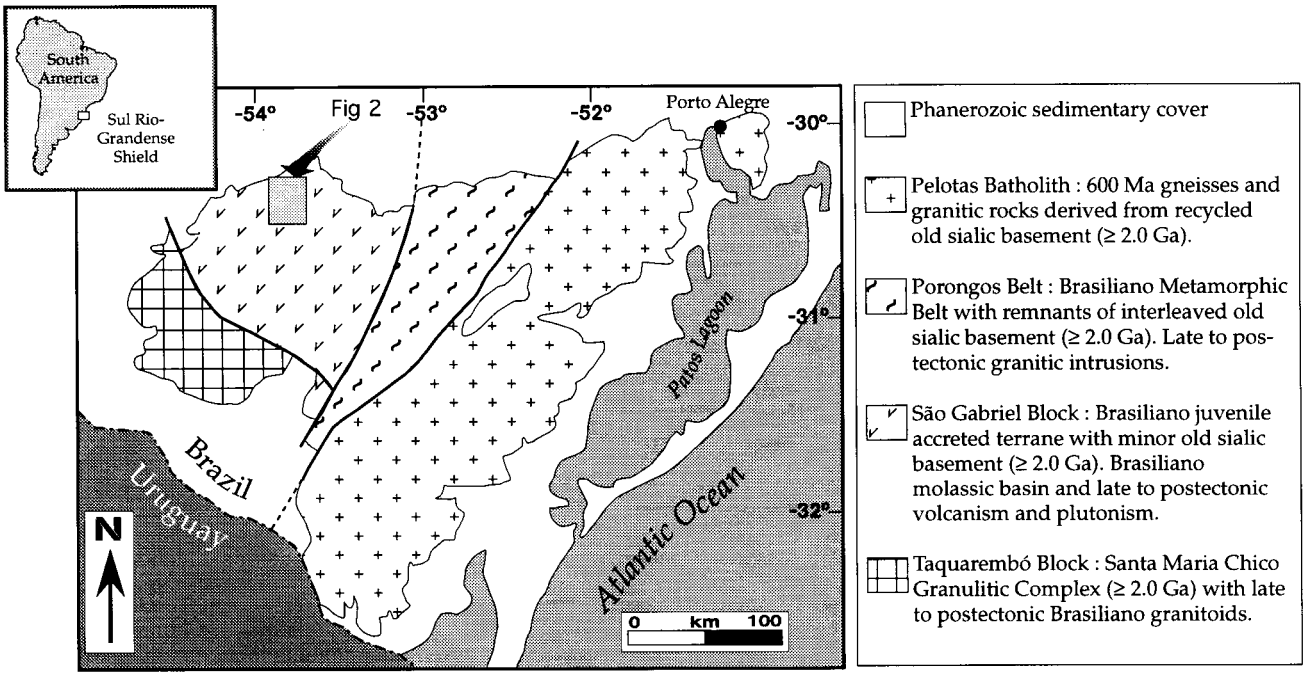

Fig. 1. Schematic geotectonic map showing the regional setting of the Bossoroca Gold Deposit in the Sul-Riograndense Shield (after Jost and Hartmann, 1984; Soliani Jr., 1986; Fragoso César et al., 1986; Babinski et al., 1996).

main deposit in the region is the Bossoroca lode-gold deposit, which has been mined for nearly seventy years. The ore occurs within quartz veins hosted by volcanic rocks of transitional low- to medium-metamorphic grade of the juvenile volcanic arc. This is a small deposit which contains a total of one ton of gold with average contents of about 15 g/ton (Koppe, 1990). The mineralisation could either be related to the regional metamorphism or to the intrusion of the nearby post-tectonic São Sepé Granite, or to a related intrusion at depth. The deposit and associated rocks were investigated in order to establish some constraints on timing and metal sources of the ore-forming event, using techniques such as sensitive high-resolution ion microprobe (SHRIMP) U/Pb isotopic determinations on zircon (129 zircon grains), Pb isotope analyses on sulfides, feldspars and whole rocks (13 samples). O and C stable isotope analyses of gangue carbonates (8 samples) were essential for constraining the source of ore fluids.

2. Geological setting

The Precambrian shield of Rio Grande do Sul State is part of the southernmost extension of the Mantiqueira Province (Hasui et al., 1975) and has four major segments (Jost and Hartmann, 1984; Soliani Jr., 1986; Fragoso César et al., 1986; Babinski et al., 1996) as shown in Fig. 1. To the east, the 600 Ma-old Pelotas Batholith, derived from crustal reworking of *ca* 2.0 Ga-old tonalite-granodiorite and metasedimentary gneisses, is juxtaposed against the 780 Ma-old Porongos schist belt to the west. The schist belt is composed of supracrustal sequences interleaved with *ca* 2.0 Ga-old basement gneisses. The western part of the shield contains the Taquarembó Block in the south and the São Gabriel Block in the north.

The Bossoroca lode-gold deposit occurs in the São Gabriel Block, near 30°S, 54°W. This block contains two major units (Fig. 2). One is the juvenile Neoproterozoic (Babinski et al., 1996) calc-alkaline volcano-plutonic island-arc association, named the Cambaí Complex for the plutonic rocks and the Vacacaí Group for the volcanic/sedimentary sequence. The other unit in this block is a late to post-tectonic volcano-plutono-sedimentary association named the Seival Association by Chemale Jr. et al. (1995), which occurs outside of the area represented in Fig. 2. Known ages are *ca* 753 Ma by Machado et al. (1990) for the Vacacaí Group (Campestre Formation) and *ca* 704 Ma by Babinski et al. (1996) for the Cambaí Complex gneisses, both using conventional zircon U/Pb geochronology. The Seival Association straddles the Precambrian/Cambrian boundary (Gresse et al., 1996).

The local andesitic rocks are mostly of pyroclastic origin and have chemical compositions rather similar to those of modern arcs. The rocks are calc alkaline, low-K and low-Nb (Koppe and Hartmann, 1988),

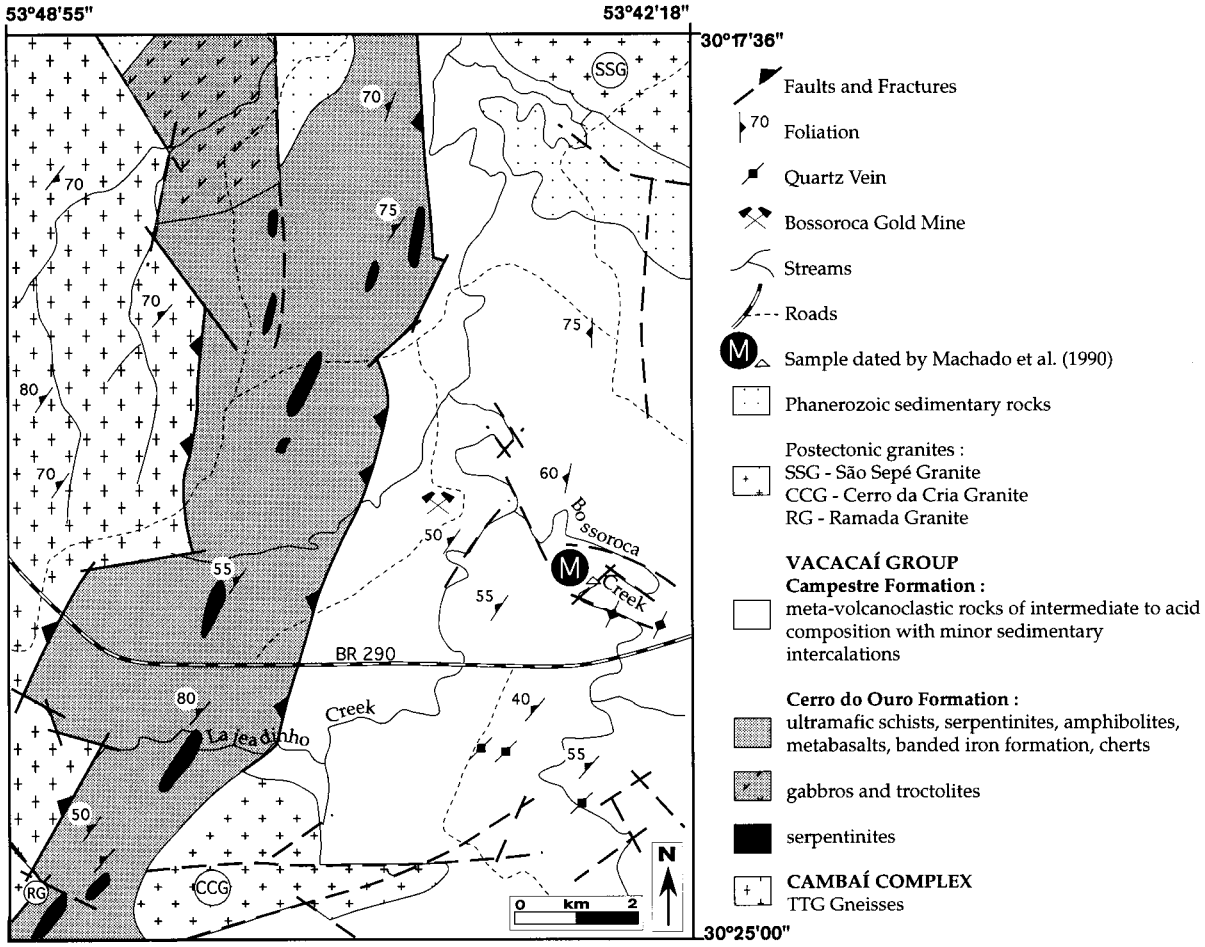

Fig. 2. Geologic map of the Bossoroca Gold Deposit district (after Koppe and Hartmann, 1988).

have a positive εNd at 750 Ma and model ages (T_{DM}) younger than 900 Ma (Babinski et al., 1996). These seem to define an old (Neoproterozoic) fragmented, subduction-related arc, which is here informally termed the Bossoroca Volcanic Arc.

The gold mineralisation occurs in the Campestre Formation, which is made up of interlayered intermediate to acid flows (rare), coarse to fine-grained tuffs (abundant), lapilli tuffs, crystal tuffs, conglomerates, sandstones, pelites and minor chert and iron formation. Intermediate to acid compositions predominate, but some basaltic rocks also occur. The magmatism is typically low-K calc-alkaline (Koppe and Hartmann, 1988).

The Cerro do Ouro Formation occurs on the western side of the Campestre Formation (Fig. 2), and contains abundant serpentinite and magnesian schist bodies interleaved with basalts, iron formations and cherts. It may be an ophiolite (Wildner, 1990), but the abundance of mafic–ultramafic volcanic rocks and the komatiitic geochemical affinity of this and regional related ultramafic units (Zarpelon, 1986; Remus, 1990; Koppe, 1990; Remus et al., 1993) is more typical of a Paleoproterozoic greenstone belt (sensu Condie, 1997) which comprises remnants blocks in the Neoproterozoic juvenile volcanic arc.

The overall structure of the rocks trends NE and dips 50° to the NW, and was probably formed by the thrusting component of a transpressive system. According to field observations, the Cambaí Complex gneisses were thrust over the Cerro do Ouro Formation, and both thrusted over the Campestre Formation. A regional metamorphic event is associated with the thrusting and varies from greenschist to middle amphibolite facies, with lower grade in the eastern part and higher grade in the western part of the area (Fig. 2). The structural evidence for thrusting is better developed in the Palma region, to the south of the mapped area. The Campestre Formation is typically altered to greenschist metamorphic grade, but in the Bossoroca deposit, the metamorphic grade reaches the transition to the amphibolite facies, with formation of hornblende in mafic schists as determined by electron microprobe analyses (Koppe, 1990). Deformation

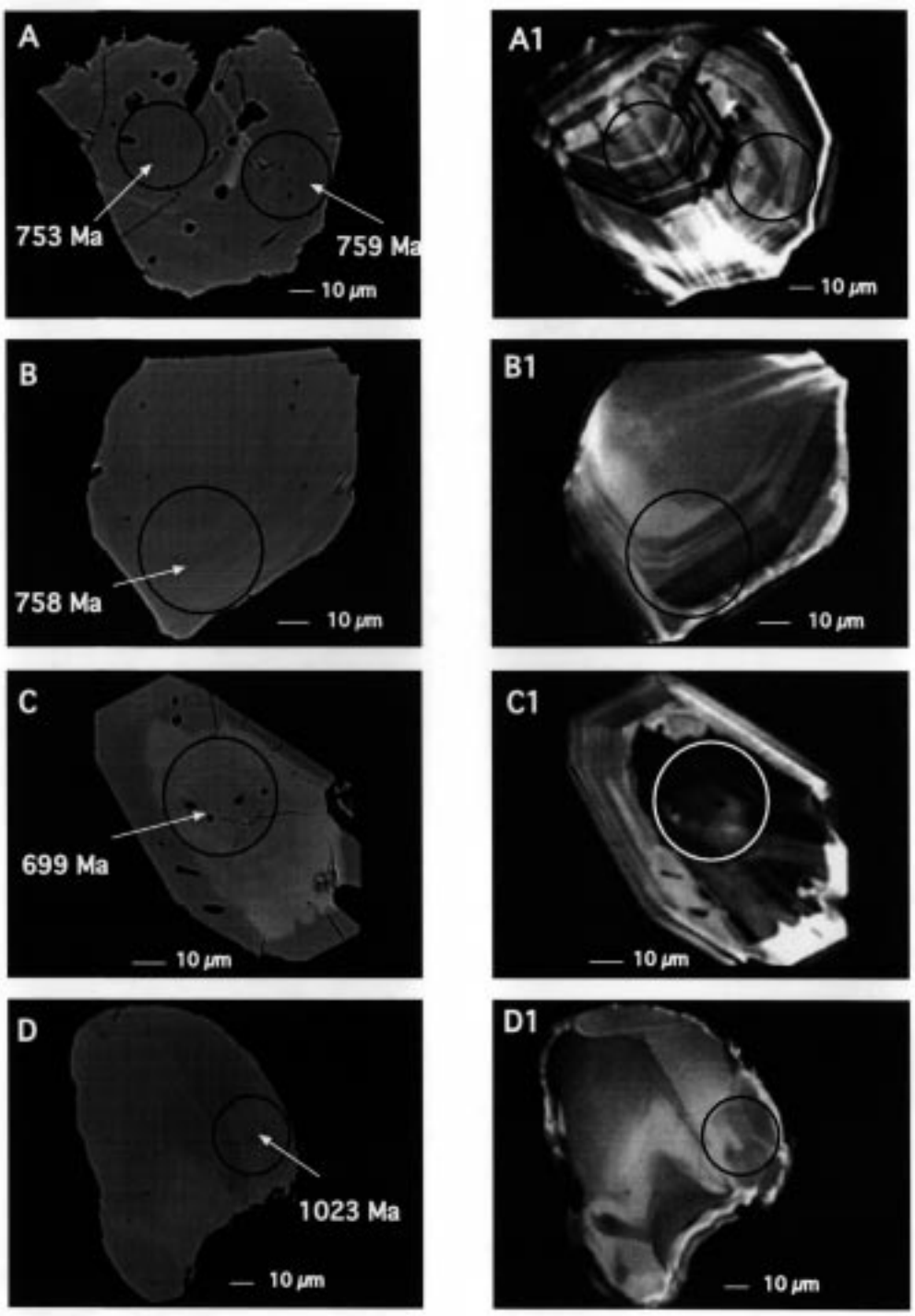

Fig. 3. SEM images of sectioned zircons from dacitic metatuff of the Campestre Formation. On the left are the BSE (backscattered electron) images, whereas CL (cathodoluminescence) images of the same grain are shown on the right. Circles indicate areas of analyses; scale bar indicated. Zircons A and B (grains 6A.9 and 6A.20) show igneous textural zonation. Zircon C (grain 6A.22) shows textural replacement of the core region, which is younger than the igneous zonation. Zircon D (grain 6A.23) is older than the magmatic event and the rounding is suggestive of inherited sedimentary zircon.

of the volcanic sequence was not very intense. The S1 schistosity or slaty cleavage, and the brittle S2 fracturing, overprinted, but did not obliterate, the sedimentary and volcanic characteristics of the rock pile. In low strain domains, the original fabrics of pyroclastic and epiclastic protoliths are very well preserved. The S1 foliation trends to the NE and dips to the NW. Local transposition of foliation is associated with the

Table 1
SHRIMP U/Pb data on zircons from dacitic metatuff of the Campestre Formation of the Vacacaí Group[a]

Grain-spot	U (ppm)	Th (ppm)	$\frac{Th}{U}$	4f206 (%)	$\frac{207^*}{206^*}$	$\frac{208^*}{206^*}$	$\frac{206^*}{238}$	$\frac{207^*}{235}$	$\frac{208^*}{232}$	%conc.	$\frac{207^*}{206}$ Age(Ma)	$\frac{206^*}{238}$ Age(Ma)	7f206 (%)
Magmatic grains													
6A.3-1	114	50	0.44	0.187	0.0649 ± 16	0.1317 ± 38	0.1248 ± 30	1.117 ± 40	0.0372 ± 14	98	773 ± 51	758 ± 17	0.241
6A.4-1	76	35	0.46	0.568	0.0618 ± 31	0.1336 ± 74	0.1255 ± 31	1.070 ± 62	0.0367 ± 22	114	667 ± 107	762 ± 17	0.226
6A.6-1	64	22	0.34	1.719	0.0676 ± 43	0.1062 ± 103	0.1283 ± 32	1.195 ± 86	0.0396 ± 40	91	856 ± 134	778 ± 18	2.015
6A.7-1	32	9	0.29	0.000	0.0688 ± 16	0.1040 ± 32	0.1261 ± 34	1.197 ± 45	0.0461 ± 20	86	893 ± 48	766 ± 19	0.494
6A.7-2	55	23	0.43	0.606	0.0684 ± 31	0.1255 ± 74	0.1228 ± 32	1.157 ± 64	0.0360 ± 23	85	880 ± 95	747 ± 18	1.114
6A.8-1	98	39	0.40	1.168	0.0593 ± 26	0.1021 ± 62	0.1219 ± 29	0.996 ± 53	0.0313 ± 21	129	576 ± 96	741 ± 17	0.602
6A.9-1	32	9	0.29	0.400	0.0679 ± 53	0.0920 ± 125	0.1250 ± 35	1.171 ± 101	0.0396 ± 55	88	867 ± 163	759 ± 20	0.812
6A.9-2	66	21	0.33	0.358	0.0658 ± 32	0.1027 ± 75	0.1240 ± 30	1.125 ± 64	0.0389 ± 30	94	800 ± 101	753 ± 17	0.534
6A.12-1	30	9	0.30	1.643	0.0600 ± 76	0.0792 ± 181	0.1239 ± 35	1.024 ± 137	0.0331 ± 77	125	602 ± 278	753 ± 20	1.120
6A.13-1	46	17	0.37	0.622	0.0684 ± 46	0.1132 ± 108	0.1252 ± 33	1.181 ± 88	0.0388 ± 39	86	880 ± 139	761 ± 19	1.080
6A.18-1	96	41	0.42	0.132	0.0659 ± 23	0.1327 ± 54	0.1275 ± 30	1.159 ± 51	0.0399 ± 19	96	805 ± 72	773 ± 17	0.250
6A.20-1	114	56	0.49	0.254	0.0625 ± 16	0.1441 ± 40	0.1248 ± 29	1.076 ± 40	0.0367 ± 14	110	691 ± 56	758 ± 17	0.012
6A.21-1	154	75	0.49	0.212	0.0652 ± 14	0.1445 ± 33	0.1222 ± 29	1.098 ± 37	0.0361 ± 12	95	779 ± 44	743 ± 16	0.346
6A.24-1	31	11	0.36	0.000	0.0718 ± 18	0.1112 ± 37	0.1229 ± 35	1.216 ± 49	0.0384 ± 18	76	979 ± 51	747 ± 20	0.920
6A.27-1	118	33	0.28	0.843	0.0612 ± 23	0.0758 ± 54	0.1211 ± 29	1.022 ± 48	0.0325 ± 25	114	647 ± 81	737 ± 16	0.528
6A.31-1	73	27	0.37	0.352	0.0650 ± 26	0.1153 ± 60	0.1300 ± 32	1.165 ± 57	0.0406 ± 24	102	776 ± 83	788 ± 18	0.308
Metamorphic/recrystallised grains													
6A.11-1	119	61	0.51	0.473	0.0603 ± 31	0.1451 ± 75	0.1157 ± 28	0.962 ± 57	0.0327 ± 19	115	615 ± 111	706 ± 16	0.159
6A.22-1	165	65	0.40	0.332	0.0633 ± 19	0.1077 ± 45	0.1144 ± 27	0.999 ± 40	0.0312 ± 15	97	718 ± 64	699 ± 15	0.401
Inherited grains/cores													
6A.15-1	54	20	0.36	0.232	0.0667 ± 29	0.1145 ± 69	0.1320 ± 33	1.213 ± 65	0.0418 ± 28	97	827 ± 92	799 ± 19	0.338
6A.23-1	132	161	1.22	0.170	0.0771 ± 13	0.3352 ± 37	0.1719 ± 40	1.828 ± 55	0.0472 ± 12	91	1124 ± 33	1023 ± 22	0.170
6A.30-1	42	15	0.36	0.000	0.0689 ± 14	0.1167 ± 30	0.1344 ± 36	1.276 ± 45	0.0431 ± 17	91	896 ± 42	813 ± 20	0.327
6A.31-2	89	30	0.33	0.000	0.0650 ± 9	0.1016 ± 19	0.1350 ± 33	1.209 ± 36	0.0416 ± 13	105	774 ± 30	816 ± 19	0.000
6A.33-1	40	15	0.38	0.000	0.0695 ± 15	0.1272 ± 33	0.1313 ± 35	1.258 ± 45	0.0437 ± 17	87	914 ± 43	795 ± 20	0.467
High common Pb													
6A.1-1	17	5	0.28	5.244	0.0373 ± 162	0.0099 ± 386	0.1220 ± 44	0.628 ± 276	0.0043 ± 166	0	0 ± 61	742 ± 25	2.186
6A.8-2	44	14	0.32	22.985	0.0511 ± 182	−0.0071 ± 434	0.1151 ± 37	0.811 ± 293	0.0000	286	245 ± 662	702 ± 21	21.894
6A.14-2	49	50	1.02	2.210	0.0564 ± 72	0.3047 ± 181	0.0926 ± 25	0.720 ± 96	0.0276 ± 18	122	468 ± 286	571 ± 15	1.893
6A.32-1	305	366	1.20	12.042	0.0592 ± 78	0.2313 ± 189	0.0628 ± 15	0.513 ± 70	0.0121 ± 10	69	573 ± 289	393 ± 9	12.529

(continued on next page)

Table 1 (*continued*)

Grain-spot	U (ppm)	Th (ppm)	Th/U	4f206 (%)	207*/206*	208*/206*	206*/238	207*/235	208*/232	%conc.	207*/206 Age(Ma)	206*/238 Age(Ma)	7f206 (%)
Pb-loss													
6A.5-1	305	202	0.66	0.293	0.0590 ± 14	0.2048 ± 37	0.0751 ± 17	0.611 ± 22	0.0232 ± 7	82	569 ± 53	467 ± 10	0.613
6A.10-1	605	28	0.05	0.251	0.0628 ± 9	0.0153 ± 19	0.0891 ± 20	0.772 ± 22	0.0297 ± 38	78	703 ± 31	550 ± 12	0.767
6A.10-2	674	49	0.07	1.217	0.0607 ± 11	0.0134 ± 25	0.1016 ± 23	0.851 ± 26	0.0187 ± 35	99	630 ± 39	624 ± 13	1.238
6A.14-1	43	33	0.77	1.011	0.0553 ± 60	0.2275 ± 151	0.0935 ± 26	0.712 ± 82	0.0275 ± 20	136	423 ± 245	576 ± 15	0.539
6A.16-1	901	250	0.28	0.068	0.0595 ± 4	0.0839 ± 9	0.0951 ± 21	0.780 ± 19	0.0288 ± 7	100	585 ± 15	585 ± 12	0.067
6A.25-1	495	339	0.68	0.001	0.0522 ± 12	0.2092 ± 32	0.0420 ± 10	0.303 ± 10	0.0129 ± 4	90	295 ± 50	265 ± 6	0.081
6A.28-1	123	39	0.32	0.000	0.0675 ± 14	0.1006 ± 29	0.0968 ± 24	0.901 ± 31	0.0306 ± 12	70	853 ± 44	596 ± 14	0.928
6A.29-1	966	311	0.32	0.633	0.0597 ± 7	0.0964 ± 16	0.0922 ± 21	0.759 ± 20	0.0276 ± 8	96	593 ± 25	569 ± 12	0.711
CZ3 (n = 10)													
Mean (wtd.)	550	30.2	0.06	0.046	0.0589	0.0172	0.0913	0.74	0.0283	102	563	564	
1 s (wtd.)	20	1.5	0.00	0.041	0.0007	0.0007	0.0021	0.02	0.0018	4	25	12	
χ^2					1.6400	1.49	1.02	1.17	1.97		1.68	0.99	

[a] SHRIMP analysis date 6/10/96. Precisions are 1 s in the last digits listed. Pb isotopic values and dates are corrected for common Pb, calculated using a Pb composition from the Cumming and Richards (1975) model at 760 Ma and the measured Pb-204. 4f206 = Proportion of Pb-206 calculated to be common Pb; %conc. = Concordance, as 100t[206*/238]/t[207*/206*].

main D1 progressive deformation episode. Brittle–ductile transcurrent shear zones concordant with the schistosity formed late in the D1 episode.

Low-pressure type, regional dynamothermal metamorphism in mafic/intermediate rocks of the Campestre Formation produced quartz + chlorite + white mica + albite + epidote + calcite assemblages in lower grade and quartz + albite + biotite + hornblende in higher grade rocks. In metapelites, the paragenesis is: quartz + muscovite + chlorite + andalusite and quartz + muscovite + biotite + albite (Zarpelon, 1986; Wildner, 1990; Koppe, 1990).

In the Bossoroca deposit, gold occurs as free gold and Au-pyrite inclusions in quartz veins of variable thicknesses. The quartz veins reach up to 1 m in thickness, but are normally around 0.3 m thick, while, in the nearby Cerrito do Ouro deposit, the quartz veins are up to 3 m thick. Veining is subparallel to the S1 schistosity, but it locally crosscuts the foliation at low angle. Veins are deformed by the D1 episode. These relationships suggest that quartz vein-related mineralisation in the area was late to syn the D1 episode. Some late quartz veins and veinlets are oblique, or perpendicular, to S1, suggesting a later generation of extensional fracturing. The gold occurs between crystals of quartz, calcite and sulfide and subordinately as inclusions or as part of the pyrite structure. Free gold is also present in many small quartz veinlets over the entire area of the volcanic arc.

The São Sepé and two other related granite plutons are intrusive into the volcano-sedimentary arc (Fig. 2), and produce metamorphic contact aureoles superimposed on low-grade regional metamorphism. Metapelites close to the São Sepé Granite contact are transformed into andalusite + staurolite + biotite + plagioclase + quartz (+ cordierite + almandine garnet) hornfels.

3. Methodology

Geological field mapping was carried out over the entire volcanic arc at the 1:50,000 scale but a more detailed 1:5,000 survey was performed on the area close to the mine (Fig. 2). The mine itself was surveyed at the 1:500 scale in several levels as stripping progressed (Koppe, 1990). Structural controls were established and rock and ore samples collected for laboratory studies.

Approximately five hundred thin sections of the entire volcanic arc were studied, followed by rock geochemistry and electron microprobe analyses of minerals (Koppe and Hartmann, 1988; Koppe, 1990). For the present investigation, rock samples were collected from the mine pit and from the São Sepé Granite. Samples weighing 1 kg were collected for Pb isotopic

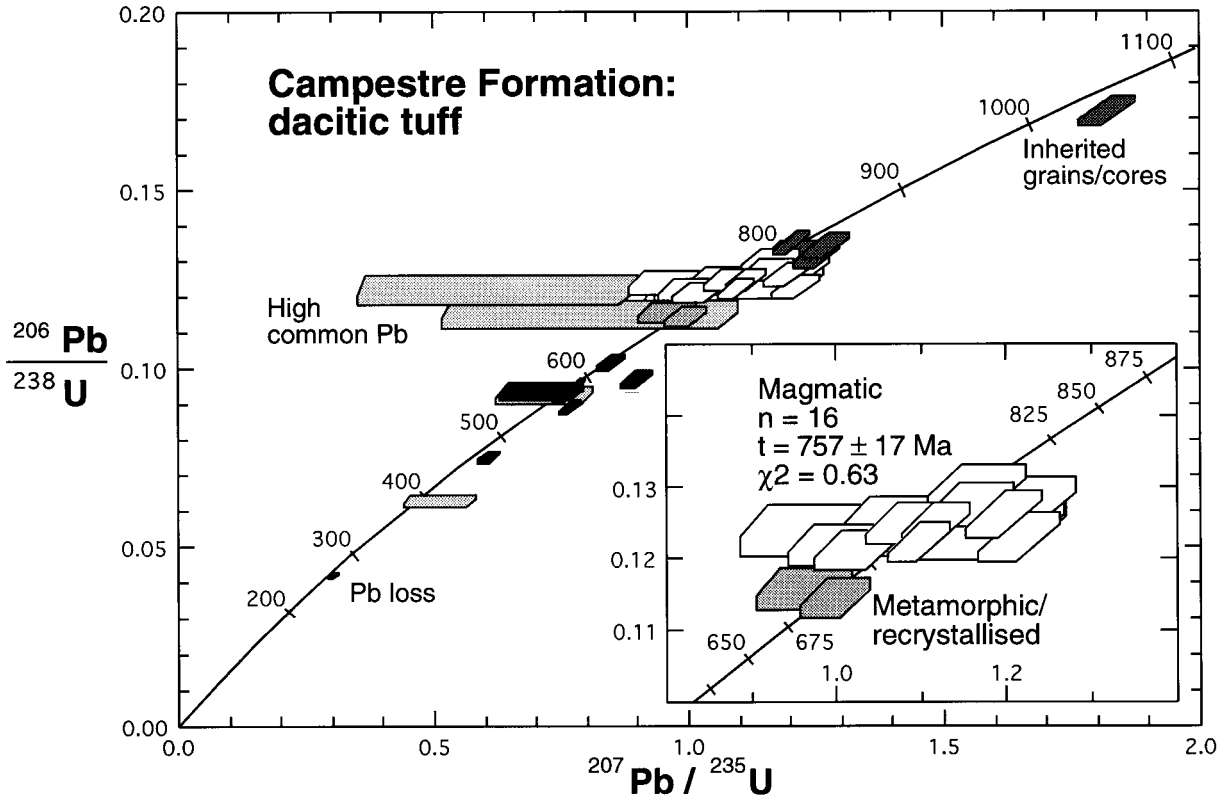

Fig. 4. Concordia diagram of zircon populations from dacitic metatuff, the host rock of the Bossoroca Gold Deposit. The main zircon population (unfilled pattern) defines the age of igneous crystallisation. The oldest zircon grain is an inherited xenocryst (medium gray pattern) and the younger grains in the detail box (light gray pattern) are the zircon population affected by metamorphism at *ca* 700 Ma. High common Pb and Pb-loss populations are discussed in the text.

studies, and about 40 kg of a dacitic crystal tuff from the mine pit were collected for zircon studies, because the rock is poor in this mineral. Only 5 kg of granite were necessary for zircon separation. Feldspars were separated from the dacite and granites by conventional magnetic and heavy liquid procedures. Ore sulfides were collected in the mine pit for sulfide Pb-isotope studies; individual sulfides were separated by hand picking.

Zircon geochronology was undertaken in one sample to determine the age of the host dacite rock from the Campestre Formation. SHRIMP investigations of zircons were undertaken at Curtin University and follow the procedures of Compston et al. (1984) and Smith et al. (1998). Scanning electron microscope images of grains to be analysed were obtained using backscattered electron (BSE) and cathodoluminescence (CL) modes at the Centre for Microscopy and Microanalysis, University of Western Australia. The dacite contained few zircons: only twenty-nine crystals were obtained and analysed from 40 kg of rock.

Rock samples for isotopic analysis were crushed and milled in an agate mortar to minimise any contamination. Lead was extracted by ion exchange chromatography at the Lead-free Laboratory, University of Western Australia, and the isotopic measurements were made on a VG354 multicollector mass spectrometer housed at Curtin University.

4. Shrimp zircon U/Pb studies

The wall-rock dacite from the open pit contains three morphological zircon types. The largest population is made up of small short prismatic, colourless, angular, commonly broken crystals. BSE/CL images (Fig. 3) reveal an internal igneous texture of oscillatory and sector zoning, most visible in the CL images. Oscilatory zoning is common in this population (Fig. 3A, 3A1). Sixteen analyses on fifteen crystals of this type (Table 1) are analytically indistinguishable from each other and show a $^{206}Pb/^{238}U$ age of 757 ± 17 Ma (Fig. 4). The U and Th contents of the zircons are low (Table 1, Fig. 5), and Th/U ratios vary from 0.2 to 0.5, which are typical of igneous zircons. The age of *ca* 757 Ma is considered to be the magmatic age of the volcanic rock, and it is in agreement with the conventional U/Pb zircon age determination of 753 ± 2 Ma

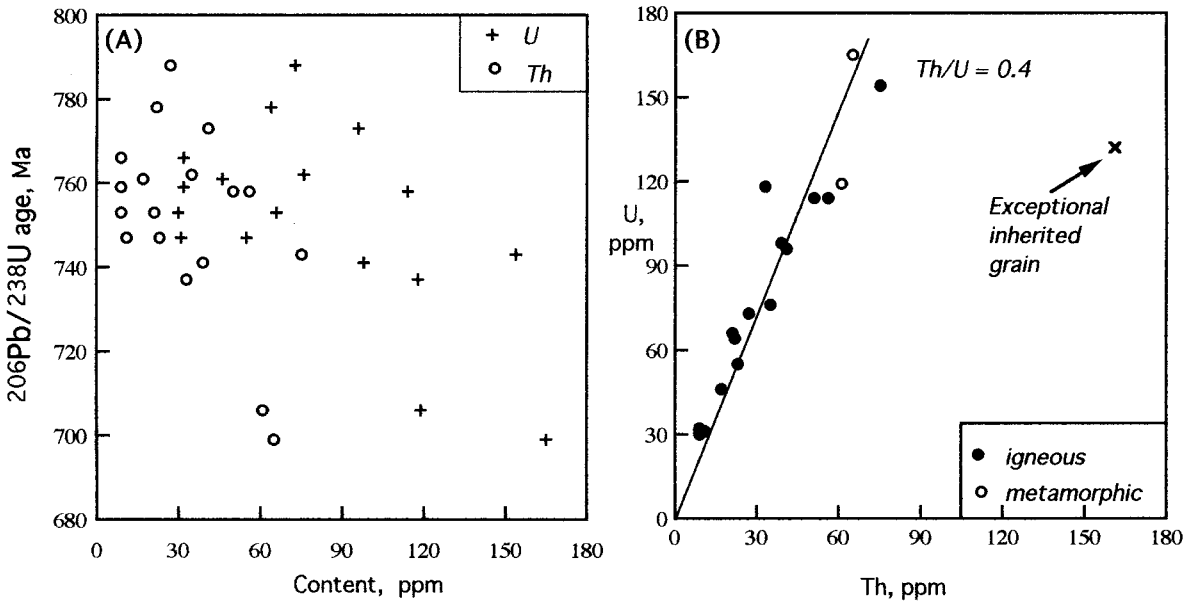

Fig. 5. $^{206}Pb/^{238}U$ age (Ma) versus U and Th (ppm) diagram showing the relatively low U and Th contents of zircons from the dacitic metatuff of the Campestre Formation (A). Th/U ratios of zircons from the dacitic metatuff showing typical ratios of igneous zircons. Th/U ratios of two metamorphic spots also shown (B).

obtained by Machado et al. (1990) for a rhyolite from the Campestre Formation (Fig. 2). A few crystals yield the same age (*ca* 757 Ma) on cores and rims (e.g., Fig. 3A), corresponding to the magmatic age. A special problem is encountered in four spots which yield ages around 800 Ma; these could be within analytical error of the 757 Ma event or else be inherited cores. In crystal 31 (Table 1), the core is 816 Ma and the rim 788 Ma. This means that the core contains inherited lead, although there are no special textural features on BSE/CL images. As a consequence, spots 31-2, 30-1, 15-1 and 33-1 are not included in the calculation of the average magmatic age.

Two zircon crystals display external forms similar to the first group, but the internal structure shows a core which is discordant to, and partly overgrows, the euhedral internal zoning (Fig. 3C, 3C1). An equivalent textural relationship of younger cores was recognised by Gebauer (1996, p. 312); this is also similar to the internal growth textures formed by fracture sealing, as described by Hartmann et al. (1997). The $^{206}Pb/^{238}U$ age of this zircon growth is 699 ± 15 Ma, which coincides with the conventional U/Pb zircon age determination of 704 ± 13 Ma on a syntectonic diorite from the nearby Cambaí Complex (Babinski et al., 1996). This *ca* 700 Ma age is considered to be the age of the M1 metamorphic event affecting the Bossoroca Arc.

One inherited crystal was identified; it is clear and shows no internal zoning; the rounding probably indicates sedimentary recycling (Fig. 3D). The $^{206}Pb/^{238}U$ age obtained is 1023 ± 22 Ma and agrees very well with previous conventional U/Pb dating of inherited zircon from a nearby rhyolite by Machado et al. (1990) (Figs. 4 and 5).

Four spot analyses have high common lead (Table 1) and have the same textural features as the magmatic population. Another group, which gives ages younger than the metamorphic event, is interpreted as a lead-loss group. These zircons lost lead, possibly due to incipient metamictization in higher U (about 900 ppm) spots and to solutions migrating through fractures.

The São Sepé Granite has two main textural facies, as characterised by field mapping, petrography and geochemistry (Sartori and Rüegg, 1979; Gastal et al., 1995). Zircons from two samples of the different granite facies were studied using the SHRIMP. The preliminary zircon date from this and another granite plutons of the São Gabriel Block were previously presented by Remus et al. (1997).

The monzogranite facies located in the northern part of pluton has a single zircon population with a $^{206}Pb/^{238}U$ age of 558 ± 8 Ma (Table 2). The magmatic zircon population is made up of yellowish to colourless euhedral prismatic and short prismatic crystals with {100} and {010} symmetric well-developed faces. BSE and CL images reveal an internal texture of massive, complex or oscillatory zoned cores and oscillatory zoned rims (Figs. 6A and B), which contain inclusions of very small long prismatic black and colorless minerals. The age of cores and rims of analysed zircons are analytically indistinguishable (Fig. 6A). The younger grains show the same texture as the main

Table 2
SHRIMP U/Pb on zircons from the monzogranite central facies of the São Sepé Granite[a]

Grain-spot	U (ppm)	Th (ppm)	$\frac{Th}{U}$	4f206 (%)	$\frac{207^*}{206^*}$	$\frac{208^*}{206^*}$	$\frac{206^*}{238}$	$\frac{207}{235}$	$\frac{208^*}{232}$	%conc.	$\frac{207^*}{206^*}$ Age(Ma)	$\frac{206^*}{238}$ Age(Ma)	7f206 (%)
Magmatic grains													
14B.1-1	228	134	0.59	0.000	0.0582 ± 12	0.1824 ± 23	0.0896 ± 14	0.719 ± 20	0.0277 ± 6	103	537 ± 45	553 ± 8	0.000
14B.2-1	335	171	0.51	0.059	0.0586 ± 12	0.1578 ± 25	0.0915 ± 14	0.740 ± 20	0.0283 ± 6	102	554 ± 46	565 ± 8	0.023
14B.2-2	128	39	0.31	0.411	0.0590 ± 26	0.0873 ± 52	0.0878 ± 15	0.714 ± 35	0.0251 ± 16	96	567 ± 97	542 ± 9	0.494
14B.3-1	277	209	0.75	0.209	0.0574 ± 18	0.2294 ± 41	0.0885 ± 14	0.701 ± 26	0.0269 ± 6	108	509 ± 69	547 ± 8	0.086
14B.4-1	249	147	0.59	0.178	0.0599 ± 18	0.1770 ± 38	0.0883 ± 14	0.729 ± 26	0.0265 ± 7	91	599 ± 65	546 ± 8	0.357
14B.5-1	227	273	1.20	0.265	0.0596 ± 21	0.3699 ± 54	0.0898 ± 14	0.738 ± 30	0.0277 ± 6	94	589 ± 77	555 ± 8	0.379
15B.1-1	341	227	0.67	0.481	0.0591 ± 13	0.2052 ± 30	0.0904 ± 22	0.737 ± 26	0.0279 ± 8	97	572 ± 49	558 ± 13	0.528
15B.4-1	1009	491	0.49	0.547	0.0593 ± 8	0.1586 ± 17	0.0916 ± 22	0.749 ± 22	0.0299 ± 8	98	577 ± 29	565 ± 13	0.584
15B.6-1	177	73	0.42	0.714	0.0582 ± 23	0.1329 ± 50	0.0940 ± 24	0.754 ± 37	0.0300 ± 14	108	538 ± 86	579 ± 14	0.578
15B.7-1	365	159	0.43	0.160	0.0577 ± 12	0.1298 ± 25	0.0926 ± 23	0.737 ± 25	0.0277 ± 9	110	519 ± 46	571 ± 13	0.000
15B.8-1	192	180	0.94	0.226	0.0579 ± 17	0.2850 ± 42	0.0936 ± 23	0.747 ± 31	0.0285 ± 8	109	527 ± 65	577 ± 14	0.064
15B.9-1	313	153	0.49	0.110	0.0579 ± 14	0.1520 ± 29	0.0894 ± 22	0.714 ± 26	0.0278 ± 9	105	527 ± 52	552 ± 13	0.027
15B.10-1	467	299	0.64	0.040	0.0580 ± 10	0.1998 ± 21	0.0893 ± 22	0.714 ± 22	0.0278 ± 7	104	530 ± 36	551 ± 13	0.000
15B.12-1	206	228	1.11	0.102	0.0593 ± 17	0.3400 ± 44	0.0929 ± 23	0.759 ± 31	0.0285 ± 8	99	578 ± 64	573 ± 14	0.121
15B.13-1	405	225	0.56	0.041	0.0601 ± 10	0.1738 ± 19	0.0931 ± 23	0.771 ± 24	0.0292 ± 8	94	607 ± 34	574 ± 13	0.154
15B.14-1	346	192	0.55	0.067	0.0582 ± 10	0.1672 ± 20	0.0919 ± 23	0.738 ± 23	0.0277 ± 8	105	539 ± 38	567 ± 13	0.000
15B.15-1	273	124	0.46	0.000	0.0605 ± 10	0.1425 ± 15	0.0919 ± 23	0.766 ± 24	0.0288 ± 8	91	621 ± 35	567 ± 13	0.182
15B.17-1	190	126	0.66	0.199	0.0573 ± 18	0.1962 ± 40	0.0904 ± 23	0.714 ± 30	0.0267 ± 9	111	502 ± 68	558 ± 13	0.017
15B.18-1	399	154	0.39	0.057	0.0576 ± 10	0.1173 ± 20	0.0923 ± 23	0.733 ± 23	0.0280 ± 8	110	515 ± 39	569 ± 13	0.000
15B.19-1	587	516	0.88	0.073	0.0585 ± 8	0.2707 ± 20	0.0915 ± 22	0.738 ± 22	0.0282 ± 7	103	548 ± 31	564 ± 13	0.020
15B.20-1	319	177	0.55	0.136	0.0579 ± 11	0.1691 ± 23	0.0943 ± 23	0.753 ± 25	0.0288 ± 8	111	525 ± 42	581 ± 14	0.000
15B.22-1	184	172	0.94	0.000	0.0581 ± 11	0.2971 ± 28	0.0938 ± 23	0.751 ± 25	0.0298 ± 8	108	533 ± 42	578 ± 14	0.000
15B.24-1	388	214	0.55	0.153	0.0599 ± 10	0.1721 ± 21	0.0911 ± 22	0.752 ± 24	0.0283 ± 8	94	599 ± 37	562 ± 13	0.276
15B.26-1	485	230	0.48	0.123	0.0575 ± 10	0.1438 ± 19	0.0893 ± 22	0.707 ± 22	0.0271 ± 8	108	509 ± 37	551 ± 13	0.000
15B.28-1	378	273	0.72	0.000	0.0603 ± 8	0.2158 ± 16	0.0930 ± 23	0.773 ± 22	0.0278 ± 7	94	613 ± 28	573 ± 13	0.133
15B.29-1	447	231	0.52	0.044	0.0594 ± 10	0.1600 ± 21	0.0901 ± 22	0.738 ± 23	0.0280 ± 8	95	583 ± 37	556 ± 13	0.133
15B.29-2	243	89	0.37	0.015	0.0590 ± 14	0.1159 ± 28	0.0892 ± 22	0.725 ± 26	0.0282 ± 10	97	566 ± 52	551 ± 13	0.065
15B.30-1	289	165	0.57	0.122	0.0581 ± 12	0.1747 ± 26	0.0913 ± 22	0.731 ± 25	0.0280 ± 8	106	532 ± 47	563 ± 13	0.021
15B.31-1	387	223	0.58	0.409	0.0598 ± 14	0.1761 ± 30	0.0900 ± 22	0.742 ± 26	0.0276 ± 8	93	596 ± 49	556 ± 13	0.542
15B.32-1	244	176	0.72	0.042	0.0604 ± 13	0.2193 ± 29	0.0901 ± 22	0.751 ± 26	0.0274 ± 8	90	619 ± 47	556 ± 13	0.255
15B.33-1	413	230	0.56	0.030	0.0593 ± 11	0.1748 ± 23	0.0924 ± 23	0.755 ± 24	0.029 ± 8	99	576 ± 40	570 ± 13	0.053
15B.34-1	629	295	0.47	0.055	0.0587 ± 7	0.1453 ± 13	0.0890 ± 22	0.720 ± 21	0.0276 ± 7	99	555 ± 26	550 ± 13	0.074
15B.35-1	342	159	0.47	0.164	0.0584 ± 12	0.1395 ± 26	0.0901 ± 22	0.726 ± 25	0.027 ± 8	102	545 ± 46	556 ± 13	0.126
15B.36-1	199	136	0.69	0.098	0.0597 ± 19	0.2135 ± 43	0.0889 ± 22	0.732 ± 31	0.0277 ± 9	93	593 ± 69	549 ± 13	0.243
15B.37-1	306	201	0.66	0.000	0.0593 ± 9	0.2024 ± 18	0.0881 ± 22	0.720 ± 22	0.0271 ± 7	94	578 ± 34	544 ± 13	0.112
15B.39-1	438	206	0.47	0.008	0.0585 ± 9	0.1450 ± 16	0.0883 ± 22	0.713 ± 22	0.0272 ± 7	99	550 ± 33	545 ± 13	0.022

(continued on next page)

Table 2 (*continued*)

Grain-spot	U (ppm)	Th (ppm)	$\frac{Th}{U}$	4f206 (%)	$\frac{207^*}{206^*}$	$\frac{208^*}{206^*}$	$\frac{206^*}{238}$	$\frac{207}{235}$	$\frac{208^*}{232}$	%conc.	$\frac{207^*}{206^*}$ Age(Ma)	$\frac{206^*}{238}$ Age(Ma)	7f206 (%)
High common Pb													
15B.25-1	506	434	0.86	2.712	0.0574 ± 22	0.2133 ± 51	0.0731 ± 18	0.579 ± 27	0.0182 ± 6	90	508 ± 82	455 ± 11	2.874
15B.34-2	166	116	0.70	2.904	0.0570 ± 41	0.1517 ± 96	0.0787 ± 20	0.618 ± 49	0.0171 ± 12	100	490 ± 160	489 ± 12	2.910
Pb loss													
15B.2-1	1965	1077	0.55	0.340	0.0586 ± 5	0.1620 ± 11	0.0843 ± 20	0.682 ± 18	0.0249 ± 6	94	554 ± 19	522 ± 12	0.444
15B.5-1	901	512	0.57	0.586	0.0598 ± 9	0.1852 ± 19	0.0808 ± 20	0.666 ± 20	0.0263 ± 7	84	596 ± 31	501 ± 12	0.896
15B.16-1	648	259	0.40	0.528	0.0592 ± 11	0.1332 ± 24	0.0807 ± 20	0.658 ± 21	0.0269 ± 8	87	574 ± 40	500 ± 12	0.768
15B.23-1	502	168	0.33	0.479	0.0590 ± 11	0.0880 ± 22	0.0798 ± 19	0.649 ± 21	0.0210 ± 7	87	567 ± 41	495 ± 12	0.711
15B.24-2	89	47	0.53	0.384	0.0564 ± 40	0.1674 ± 92	0.0821 ± 22	0.639 ± 50	0.0261 ± 16	108	470 ± 158	509 ± 13	0.262
15B.27-1	623	325	0.52	0.597	0.0589 ± 11	0.1725 ± 24	0.0782 ± 19	0.635 ± 21	0.0259 ± 7	86	562 ± 41	485 ± 11	0.844
15B.38-1	564	274	0.49	0.407	0.0592 ± 11	0.1540 ± 24	0.0844 ± 21	0.690 ± 22	0.0268 ± 8	91	575 ± 41	523 ± 12	0.580
Discordant outlier													
15B.22-2	112	84	0.75	0.000	0.0641 ± 15	0.2345 ± 32	0.0914 ± 23	0.808 ± 30	0.0287 ± 8	76	746 ± 51	564 ± 14	0.640
CZ3 (n = 17)													
Mean (wtd.)	550	30.1	0.06	0.055	0.0589	0.0169	0.0914	0.743	0.0283	99	565	564	0.074
1 s (wtd.)	10	0.7	0.06	0.001	0.0007	0.0012	0.0020	0.018	0.0021	5	24	12	0.074
χ^2					0.62	0.92	0.09	0.92	1.02		0.63		0.92

[a] SHRIMP analysis dates 2/5/96 and 17/5/96. Precisions are 1 s in the last digits listed. Pb isotopic values and dates are corrected for common Pb, calculated using a Pb composition from the Cumming and Richards (1975) model at 560 Ma and the measured Pb-204. 4f206 = Proportion of Pb-206 calculated to be common Pb; %conc. = Concordance, as 100t[$206^*/238$]/t[$207^*/206^*$].

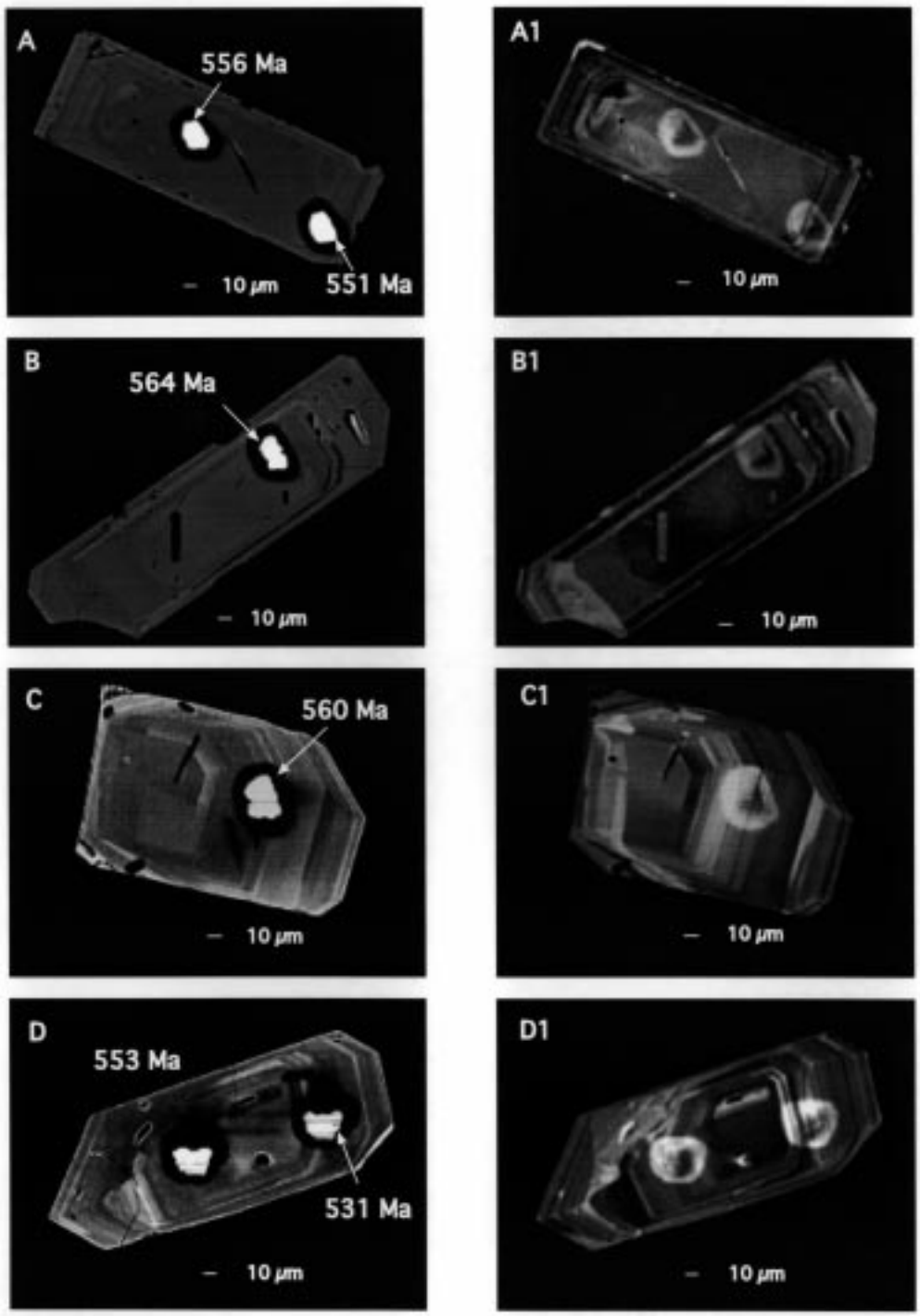

Fig. 6. SEM images of sectioned zircons from the São Sepé Granite. The images on the left are BSE, whereas CL images of the same grains are shown on the right. Marks indicate areas of analysis; scale bar indicated. Zircons A and B (grains 15B.29 and 15B.19) are from the monzogranite central facies, zircons C and D (grains 15A.33 and 15A.22) are from the microgranite border facies.

magmatic population. These zircons lost lead due to modern weathering or contain high common lead (Fig. 7, Table 2).

The sample from the microgranite facies was collected from a quarry at the SE edge of the pluton, and has only one distinctive magmatic zircon population. It is represented by colourless and yellowish grains of prismatic and short prismatic zircons with symmetrical and asymmetrical {101} and {110} pyramid faces, and has a $^{206}Pb/^{238}U$ age of 550 ± 6 Ma (Fig. 8 and Table 3) which is interpreted as the magmatic age of this granite border facies. BSE and CL images show an in-

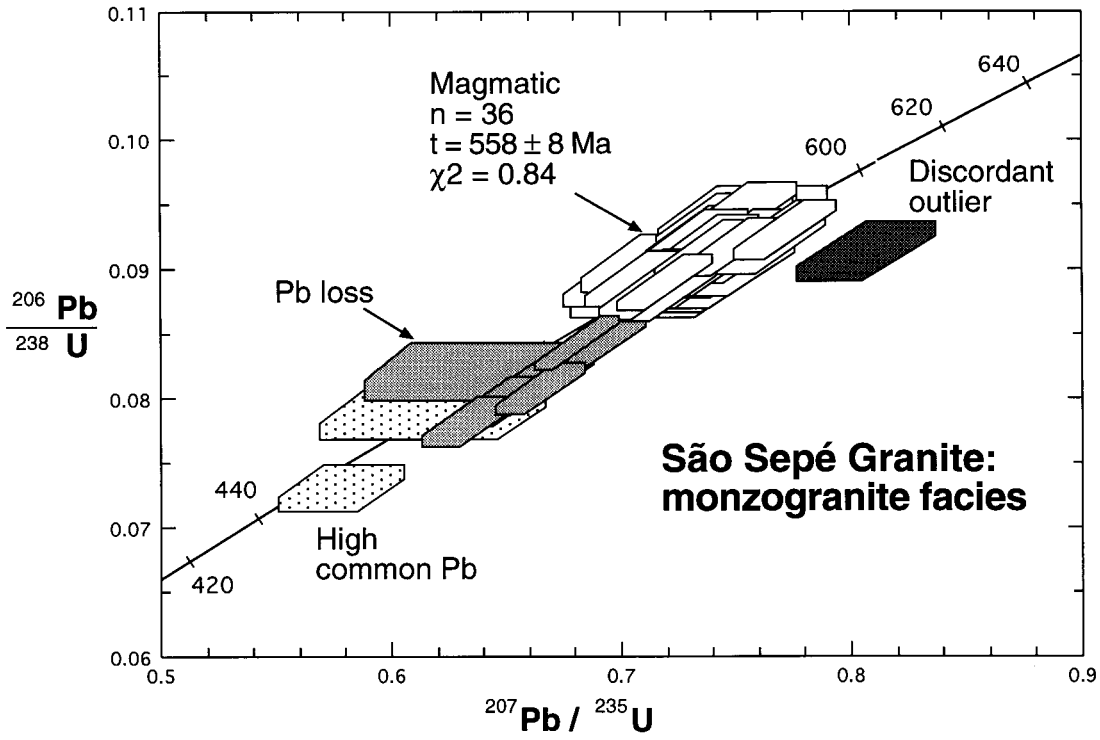

Fig. 7. Concordia diagram of zircon populations from the monzogranite central facies of the São Sepé Granite pluton. The main zircon group (unfilled pattern) defines the magmatic age of the central facies of the pluton. The younger zircon populations refer to a high common Pb (stippled pattern) and to the zircons that lost Pb due to modern weathering (medium gray pattern).

ternal texture of massive or oscillatory and, rarely, complex zoned cores. Oscillatory zoning is visible especially in the rims of grains (Figs. 6C, D). The discordant Th–U–Pb zircon group and high common Pb group (Fig. 8) have the same morphologic characteristics as the magmatic population. A value of εNd of −10 for the microgranite facies, and a model age (T_{DM}) of 2.3 Ga, indicate its derivation from ancient crustal rocks (Remus et al., 1997). Older zircon xenocrysts are absent in this granite, and this may be due to the high temperature of the magma, which is likely to have caused complete dissolution of older zircons derived from the basement rocks of the granite source region. This evidence, and Pb and Nd isotopic data, indicate an old crustal source origin (possibly granulites) for the granite which is compared to A-type granites and agrees well with previous geochemical classification (Gastal et al., 1995).

5. Fluids

Fluid inclusion studies in quartz veins by Koppe (1990) indicate an average temperature of gold deposition of 247°C and a lithostatic pressure ranging from 500 to 1300 bars. The fluid composition is represented by the H_2O–CO_2 system with low salinity (about 1% NaCl equiv.) and average density of 0.82 g/cm^3. $\delta^{13}C$ values for gangue calcite are between −5.6 and −8.2‰ PDB (n = 8), whereas $\delta^{18}O$ values fall between +15 and +16.7‰ SMOW (n = 8). This indicates a homogeneous fluid and stable conditions of temperature and pressure during mineralisation. The data suggest that the ore fluid was a deeply derived fluid (Groves et al., 1992). Fluids probably ascended through regional shear zone structures and reached the registered transitional greenschist/amphibolite facies position in the upper crust (Koppe, 1990).

6. Lead isotopes and source of mineralisation

Lead isotopic analyses were performed on several minerals and rocks in order to assess the source of Pb in the mineralising system. Galenas from the main gold-quartz vein in the Bossoroca Mine pit were analysed. Analyses were also done on plagioclase and whole-rock samples from the wall-rock dacite, and also on K-feldspars from two facies of the São Sepé Granite. The feldspars were separated and analysed because their low U/Pb allowed the Pb isotope composition to better reflect the initial Pb in the granites (e.g., McNaughton and Bickle, 1987). The lead isotopic data are presented in Table 4, and shown on a

Table 3
SHRIMP U/Pb data on zircons from the microgranite border facies of the São Sepé Granite[a]

Grain-spot	U (ppm)	Th (ppm)	$\frac{Th}{U}$	4f206 (%)	$\frac{207^*}{206^*}$	$\frac{208^*}{206^*}$	$\frac{206^*}{238}$	$\frac{207^*}{235}$	$\frac{208^*}{232}$	%conc.	$\frac{207^*}{206^*}$ Age(Ma)	$\frac{206^*}{238}$ Age(Ma)	7f206 (%)
Magmatic													
14A.1-1	57	40	0.70	0.354	0.0613 ± 53	0.2170 ± 124	0.0870 ± 16	0.736 ± 67	0.0268 ± 16	83	651 ± 186	538 ± 9	0.736
14A.4-1	55	48	0.87	0.293	0.0622 ± 54	0.2464 ± 127	0.0859 ± 16	0.737 ± 67	0.0244 ± 14	78	683 ± 185	531 ± 9	0.807
14A.5-1	63	32	0.50	0.767	0.0567 ± 50	0.1431 ± 113	0.0888 ± 16	0.694 ± 64	0.0252 ± 21	114	480 ± 195	548 ± 9	0.551
14A.6-1	122	54	0.45	0.000	0.0609 ± 16	0.1435 ± 26	0.0889 ± 13	0.746 ± 24	0.0286 ± 7	86	636 ± 57	549 ± 7	0.295
14A.9-1	215	109	0.51	0.598	0.0585 ± 21	0.1561 ± 45	0.0901 ± 12	0.726 ± 29	0.0276 ± 9	102	547 ± 78	556 ± 7	0.570
14A.10-1	633	360	0.57	0.059	0.0588 ± 8	0.1754 ± 16	0.0876 ± 10	0.709 ± 14	0.0270 ± 4	97	558 ± 30	541 ± 6	0.115
14A.11-1	211	123	0.58	0.146	0.0586 ± 16	0.1784 ± 35	0.0931 ± 12	0.753 ± 24	0.0285 ± 7	104	554 ± 61	574 ± 7	0.080
14A.12-1	108	86	0.79	0.130	0.0556 ± 27	0.2438 ± 64	0.0903 ± 14	0.692 ± 37	0.0278 ± 9	128	437 ± 109	557 ± 8	0.000
14A.13-1	349	178	0.51	0.342	0.0568 ± 15	0.1393 ± 31	0.0882 ± 11	0.691 ± 21	0.0240 ± 6	112	486 ± 58	545 ± 6	0.152
15A.6-1	338	369	1.09	0.392	0.0610 ± 14	0.3234 ± 34	0.0860 ± 18	0.724 ± 24	0.0254 ± 6	83	641 ± 48	532 ± 11	0.758
15A.7-1	145	73	0.50	0.518	0.0549 ± 24	0.1483 ± 52	0.0893 ± 20	0.676 ± 34	0.0263 ± 11	135	408 ± 96	551 ± 12	0.069
15A.8-1	178	97	0.55	0.093	0.0577 ± 19	0.1654 ± 41	0.0873 ± 19	0.694 ± 29	0.0263 ± 9	104	518 ± 72	539 ± 11	0.025
15A.9-1	118	121	1.03	0.254	0.0592 ± 25	0.3246 ± 62	0.0910 ± 20	0.743 ± 37	0.0288 ± 9	98	574 ± 92	562 ± 12	0.295
15A.9-2	125	53	0.42	0.387	0.0560 ± 26	0.1226 ± 56	0.0911 ± 20	0.704 ± 38	0.0264 ± 14	124	453 ± 102	562 ± 12	0.041
15A.11-1	221	106	0.48	0.355	0.0568 ± 18	0.1401 ± 38	0.0882 ± 19	0.691 ± 28	0.0257 ± 9	112	485 ± 70	545 ± 11	0.162
15A.12-1	861	393	0.46	0.004	0.0587 ± 6	0.1391 ± 11	0.0897 ± 19	0.726 ± 18	0.0273 ± 6	100	554 ± 23	554 ± 11	0.006
15A.14-1	66	94	1.43	0.333	0.0571 ± 42	0.4448 ± 112	0.0874 ± 21	0.688 ± 55	0.0272 ± 10	109	494 ± 164	540 ± 12	0.185
15A.15-1	163	84	0.52	0.000	0.0615 ± 13	0.1605 ± 22	0.0892 ± 19	0.757 ± 25	0.0277 ± 7	84	658 ± 46	551 ± 11	0.365
15A.16-1	445	535	1.20	0.248	0.0585 ± 10	0.3554 ± 27	0.0885 ± 19	0.714 ± 21	0.0261 ± 6	100	549 ± 39	547 ± 11	0.257
15A.17-1	178	65	0.37	0.100	0.0563 ± 19	0.1085 ± 39	0.0897 ± 19	0.697 ± 29	0.0266 ± 11	119	465 ± 74	554 ± 12	0.000
15A.19-1	132	59	0.45	0.000	0.0584 ± 15	0.1443 ± 25	0.0893 ± 20	0.719 ± 26	0.0286 ± 8	102	543 ± 57	552 ± 12	0.000
15A.22-1	161	108	0.67	0.315	0.0572 ± 20	0.1998 ± 45	0.0896 ± 20	0.706 ± 31	0.0268 ± 9	111	497 ± 78	553 ± 12	0.134
15A.22-2	166	62	0.37	0.334	0.0578 ± 19	0.1075 ± 38	0.0859 ± 19	0.685 ± 29	0.0248 ± 10	101	524 ± 74	531 ± 11	0.310
15A.26-1	258	534	2.07	0.125	0.0575 ± 17	0.6430 ± 56	0.0881 ± 19	0.698 ± 27	0.0273 ± 6	107	510 ± 65	544 ± 11	0.016
15A.27-1	173	133	0.77	0.000	0.0604 ± 13	0.2409 ± 27	0.0927 ± 20	0.772 ± 25	0.0290 ± 7	92	618 ± 45	571 ± 12	0.160
15A.28-1	238	113	0.48	0.235	0.0583 ± 15	0.1404 ± 31	0.0909 ± 19	0.730 ± 26	0.0268 ± 8	104	539 ± 57	561 ± 12	0.164
15A.29-1	123	93	0.75	0.000	0.0594 ± 15	0.2257 ± 31	0.0926 ± 21	0.758 ± 27	0.0277 ± 7	98	581 ± 54	571 ± 12	0.033
15A.30-1	373	261	0.70	0.000	0.0599 ± 9	0.2159 ± 18	0.0891 ± 19	0.736 ± 20	0.0274 ± 6	91	601 ± 31	550 ± 11	0.171
15A.31-1	145	74	0.51	0.246	0.0600 ± 26	0.1535 ± 59	0.0912 ± 20	0.754 ± 39	0.0275 ± 12	93	604 ± 95	562 ± 12	0.384
15A.32-1	184	117	0.64	0.000	0.0566 ± 14	0.1966 ± 27	0.0888 ± 19	0.693 ± 24	0.0274 ± 7	115	477 ± 54	548 ± 11	0.000
15A.33-1	103	71	0.69	0.105	0.0582 ± 30	0.2046 ± 70	0.0907 ± 21	0.729 ± 43	0.0270 ± 11	104	539 ± 114	560 ± 12	0.036
15A.34-1	181	76	0.42	0.000	0.0590 ± 12	0.1284 ± 18	0.0865 ± 22	0.704 ± 24	0.0263 ± 8	94	569 ± 44	535 ± 13	0.111
15A.35-1	218	115	0.53	0.189	0.0571 ± 17	0.1629 ± 38	0.0876 ± 22	0.690 ± 29	0.0270 ± 9	109	496 ± 67	541 ± 13	0.044
15A.36-1	290	162	0.56	0.034	0.0588 ± 13	0.1719 ± 27	0.0888 ± 22	0.720 ± 25	0.0274 ± 8	98	560 ± 48	548 ± 13	0.072
15A.38-1	139	102	0.73	0.205	0.0589 ± 22	0.2118 ± 49	0.0917 ± 23	0.745 ± 35	0.0265 ± 9	101	563 ± 80	566 ± 14	0.195

(continued on next page)

Table 3 (*continued*)

Grain-spot	U (ppm)	Th (ppm)	$\frac{Th}{U}$	4f206 (%)	$\frac{207^*}{206^*}$	$\frac{208^*}{206^*}$	$\frac{206^*}{238}$	$\frac{207^*}{235}$	$\frac{208^*}{232}$	%conc.	$\frac{207^*}{206^*}$ Age(Ma)	$\frac{206^*}{238}$ Age(Ma)	7f206 (%)
High common Pb													
14A.3-1	180	238	1.32	0.566	0.0642 ± 29	0.4005 ± 73	0.0869 ± 12	0.769 ± 37	0.0264 ± 6	72	747 ± 94	537 ± 7	1.295
14A.7-1	254	321	1.26	1.117	0.0573 ± 25	0.3500 ± 63	0.0805 ± 10	0.636 ± 30	0.0224 ± 5	99	502 ± 96	499 ± 6	1.125
14A.8-1	232	50	0.22	1.454	0.0569 ± 28	0.0705 ± 62	0.0901 ± 12	0.706 ± 37	0.0293 ± 26	114	487 ± 109	556 ± 7	1.233
14A.14-1	182	88	0.48	3.995	0.0651 ± 44	0.1692 ± 102	0.0958 ± 13	0.860 ± 61	0.0336 ± 21	76	777 ± 143	590 ± 8	4.638
14A.16-1	55	48	0.88	2.601	0.0589 ± 87	0.2736 ± 210	0.0869 ± 17	0.706 ± 107	0.0270 ± 22	95	563 ± 326	537 ± 10	2.684
15A.18-1	92	125	1.35	4.387	0.0646 ± 67	0.2460 ± 160	0.0912 ± 22	0.811 ± 89	0.0166 ± 12	74	760 ± 222	562 ± 13	5.054
15A.21-1	126	220	1.74	7.947	0.0526 ± 76	0.3010 ± 184	0.0764 ± 18	0.555 ± 83	0.0132 ± 9	152	313 ± 300	475 ± 11	7.503
15A.24-1	75	70	0.94	11.548	0.0480 ± 109	0.2214 ± 260	0.0885 ± 23	0.586 ± 135	0.0209 ± 25	543	101 ± 462	547 ± 13	10.416
15A.25-1	165	251	1.52	43.049	0.0479 ± 177	0.4796 ± 434	0.0881 ± 25	0.582 ± 218	0.0278 ± 26	564	96 ± 699	544 ± 15	42.319
Discordant U-Th-Pb													
14A.2-1	531	303	0.57	0.265	0.0590 ± 12	0.1368 ± 25	0.0878 ± 10	0.714 ± 18	0.0210 ± 5	96	566 ± 44	542 ± 6	0.343
15A.13-1	201	177	0.88	0.134	0.0607 ± 20	0.1592 ± 43	0.0843 ± 18	0.706 ± 29	0.0152 ± 5	83	630 ± 70	522 ± 11	0.496
15A.20-1	332	154	0.46	0.465	0.0573 ± 15	0.1095 ± 32	0.0846 ± 18	0.668 ± 24	0.0200 ± 7	104	502 ± 58	524 ± 11	0.396
15A.37-1	134	137	1.03	0.156	0.0587 ± 26	0.1893 ± 60	0.0842 ± 21	0.681 ± 37	0.0155 ± 6	94	556 ± 98	521 ± 13	0.271
CZ3 (n = 36)													
Mean (wtd.)	550	30.2	0.06	0.059	0.0590	0.0167	0.0914	0.744	0.0278	100	567	564	0.080
1 s (wtd.)	14	1	0.00	0.048	0.0007	0.0011	0.0017	0.017	0.0018	5	27	10	0.070
χ^2					0.77		0.91	0.83	1.97		0.77	0.98	

[a] SHRIMP analysis dates 29/4/96, 2/5/96 and 17/5/96. Precisions are 1 s in the last digits listed. Pb isotopic values and dates are corrected for common Pb, calculated using a Pb composition from the Cumming and Richards (1975) model at 560 Ma and the measured Pb-204. 4f206 = Proportion of Pb-206 calculated to be common Pb; %conc. = Concordance, as 100t[206*/238]/t[207*/206*].

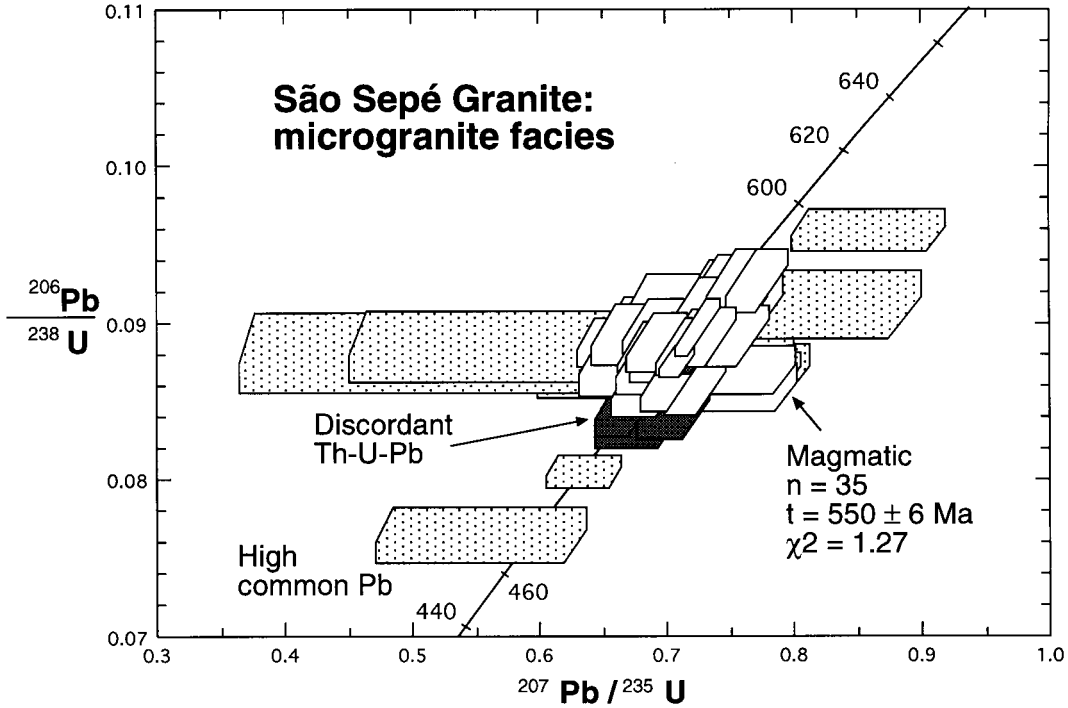

Fig. 8. Concordia diagram of zircon populations from the microgranite border facies of the São Sepé Granite pluton. The main zircon group (unfilled pattern) defines the magmatic age of the border facies of the pluton. The younger zircons close to the magmatic population refer to a discordant Th–U–Pb group (gray pattern). The high common-Pb zircons are stippled.

common lead diagram in Fig. 9. The plagioclase and two volcanic samples plot on a Pb–Pb isochron compatible with a *ca* 750 Ma age of igneous crystallisation, as determined by SHRIMP. The third sample plots off the isochron, probably because it is more altered and enriched in tourmaline (~2 wt%).

The galena data, which are considered the best estimates of the initial Pb composition in the ore system, are isotopically homogeneous and also plot on the *ca* 750 Ma reference isochron. Although the galena–plagioclase–metadacite array of data could be interpreted as galena formation shortly after volcanism, the slope of the reference isochron is relatively insensitive to age. The quartz vein-related mineralisation is considered to be late in the D1-M1 episode at *ca* 700 Ma, based on field observations. This is the suggested age of deposition of gold in the Bossoroca Mine. The deposits in the area appear to be restricted to the 750–700 Ma interval. The Pb isotope data are compatible with the timing constraints. Further, the Pb in galenas from the Bossoroca deposit is also compatible with derivation solely from the host metadacites at *ca* 700 Ma.

Lead isotopic data for K-feldspars from the border facies and core facies of the São Sepé granitic rocks are shown in Fig. 9. The average of the least radiogenic Pb from K-feldspars from each facies of the granite is the best estimate for the initial Pb isotopic compositions of the magma. These compositions for the two facies are similar to each other, but distinctly more primitive than the galena data (Fig. 9). This large contrast in Pb isotopic composition is distinctive. Thus, a granite of similar isotopic characteristics and age to the São Sepé Granite could not have contributed Pb to the mineralising fluid. Even a small contribution would have caused the galena data to fall below the 750 Ma reference isochron in Fig. 9.

The Pb isotope data show that the ore fluids in the Bossoroca gold deposit were probably derived from the host terrane or the source rock of host terrane. The structural timing of mineralisation was late in the metamorphic cycle, and this deposit is considered to be an epizonal orogenic gold deposit in the sense of Groves et al. (1998). It is inferred that metals were mobilised by fluids ascending through the Campestre Formation volcanic pile. These ascending fluids scavenged lead and gold to deposit the metals in structurally controlled sites higher in the crust. Also, the metals could be derived from the same deep source region of volcanic rocks of Campestre Formation. The main source of fluids most probably was the deeper crust.

7. Conclusions

SHRIMP U/Pb dating of zircons from dacitic wall-

Table 4
Lead isotope data from lode gold quartz of Bossoroca Deposit, Campestre Formation and São Sepé Granite border and central facies

Sample number	Geologic unit	Lithologic unit	Sample type	206Pb/204Pb	207Pb/204Pb	208Pb/204Pb
GA-1	Bossoroca lode	Quartz vein	Galena	17.465	15.458	37.112
GA-2	Bossoroca lode	Quartz vein	Galena	17.468	15.460	37.130
GA-0	Bossoroca lode	Quartz vein	Galena	17.476	15.465	37.126
EBL-3	Campestre Formation	Dacitic metatuff	Plagioclase	17.692	15.471	37.171
EB	Campestre Formation	Dacitic metatuff	Whole rock	18.502	15.560	37.802
EB2	Campestre Formation	Dacitic metatuff	Whole rock	18.292	15.502	37.438
EB3	Campestre Formation	Dacitic metatuff	Whole rock	18.518	15.524	37.675
ASS	São Sepé Granite-border	Microgranite	k-feldspar	15.397	15.029	35.860
A2	São Sepé Granite-border	Microgranite	k-feldspar	15.387	15.038	35.849
A3	São Sepé Granite-border	Microgranite	k-feldspar	15.552	15.016	35.842
BSS	São Sepé Granite-central	Monzogranite	k-feldspar	15.302	15.007	35.827
B1	São Sepé Granite-central	Monzogranite	k-feldspar	15.190	15.011	35.808
B2	São Sepé Granite-central	Monzogranite	k-feldspar	15.184	15.003	35.829

rocks of the Campestre Formation, which host the Bossoroca lode-gold deposit, yields an age of 757 ± 17 Ma for volcanism which formed this part of the juvenile island arc. The age of the peak of metamorphism for the Campestre Formation is estimated to be *ca* 700 Ma, based on SHRIMP age data on 757 Ma zircons which show textural re-equilibration. The structural timing of the ores is compatible with the younger age, which is also the age of mineralisation. Lead isotope evidence suggests that the Pb in the ore fluid was derived from the host Campestre Formation or its source region.

The São Sepé Granite intruded the volcanic arc at *ca* 550 Ma and caused a marked metamorphic contact aureole on rocks of the Campestre Formation. However, the initial Pb composition of granite samples is markedly different from the initial Pb of the Bossoroca ore, showing that the granite, or a related magma at depth, could not be the source of the metals in the gold deposit.

This study indicates that metals concentrated in the Bossoroca lode-gold deposit were mobilised during regional dynamothermal metamorphism by deeply derived fluids that ascended through the volcano/

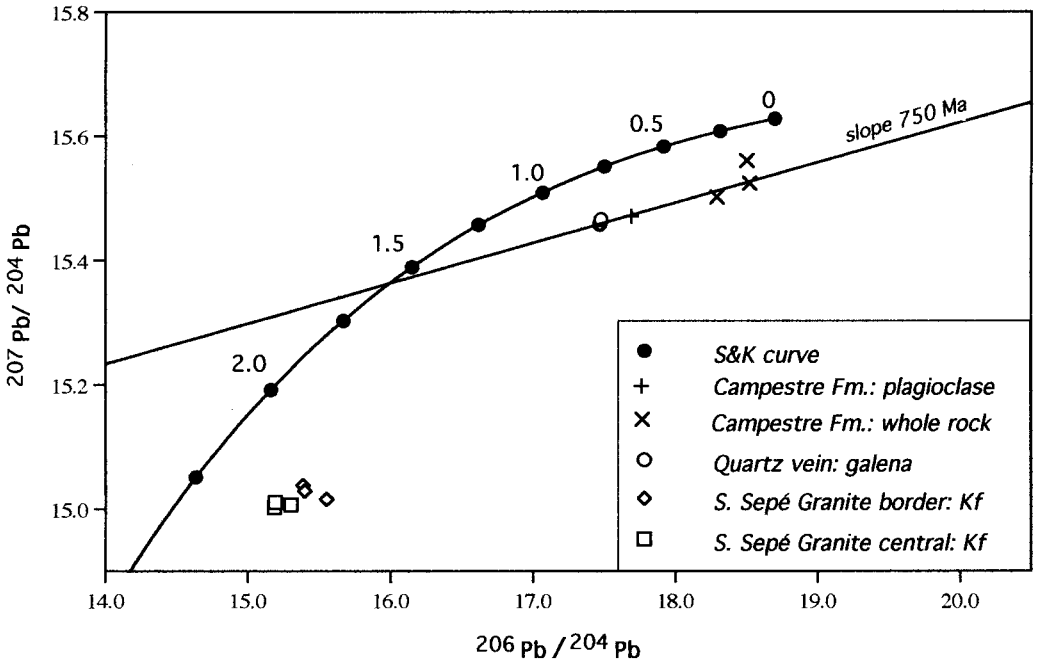

Fig. 9. Common-lead isotope diagram showing the Campestre Formation (dacite) whole-rocks and plagioclase, and galenas from quartz gold veins of the Bossoroca Gold Deposit. K-feldspars from the border and central facies of the São Sepé Granite are also shown for comparison. The 750 Ma reference isochron for the Campestre Formation and the Stacey and Kramers (1975) growth curve are shown for reference.

sedimentary Campestre Formation, scavenged lead and gold, and later deposited the metals in structurally controlled sites at higher crustal levels. Also the metals could be derived from the same deep source region of volcanic rocks of Campestre Formation. The O-C stable isotope evidence is compatible with a deeply derived ore fluid.

Acknowledgements

This paper is part of a PhD study on the Copper Province of Rio Grande do Sul funded by CNPq-National Research Council of Brazil to the first author (Grant 201393/94-8). Zircon analyses were carried out on a SHRIMP II operated by a consortium consisting of Curtin University of Technology, the Geological Survey of Western Australia and the University of Western Australia with the support of the Australian Research Council. We thank Marion Dahl (UWA-Australia) for help with the analytical data and Dra. Tamar Galembeck (UNESP-SP) for the preliminary zircon sample preparation. Paul Potter reviewed the English version of the paper. Critical reviews by Dr. M.M. Pimentel and H.E. Gaudette greatly improved the manuscript.

References

Babinski, M., Chemale Jr, F., Hartmann, L.A., Van Schmus, W.R., Silva, L.C., 1996. Juvenile accretion at 750–700 Ma in southern Brazil. Geology 24 (5), 439–442.

Compston, W., Williams, I.S., Meyer, C., 1984. U-Pb geochronology of zircons from Lunar breccia 73217 using a sensitive high-mass resolution ion microprobe. Journal of Geophysical Research 89 (Suppl.), B525–B534.

Condie, K.C., 1997. Plate Tectonics and Crustal Evolution, 4th ed. Butterworth-Heinemann, Oxford, 282 pp.

Chemale Jr, F., Hartmann, L.A., Silva, L.C., 1995. Stratigraphy and tectonism of Precambrian to Early Paleozoic units of southern Brazil and Uruguay. Excursion Guidebook. Acta Geologica Leopoldensia 42 (XVIII), 5–117.

Cumming, G.L., Richards, J.R., 1975. Ore lead isotope ratios in a continuously changing Earth. Earth and Planetary Science Letters 28, 155–178.

Fragoso César, A.R.S., Figueiredo, M.C.H., Soliani Jr, E., Faccini, U.F., 1986. O Batólito de Pelotas (Proterozóico Superior/Eo-Paleozóico) no Escudo do Rio Grande do Sul. In: Congresso Brasileiro de Geologia, 34, Goiânia, Anais, vol. 3, pp. 167–191.

Gastal, M.C., Nardi, L.V.S., Lafon, J.M. 1995. Classifiçáó dos granito\acute\ides pertencentes a suite intrusiva Saibro (SIS), RS Simpo\acute\sio Sul-Brasileiro de Geologia, 6, Porto Alegre, Resumos Expandidos, 72–76.

Gebauer, D., 1996. A P-T-t path for (ultra-?) high-pressure ultramafic/mafic rock-association and its felsic country-rocks based on SHRIMP-dating of magmatic and metamorphic zircon domains: Alpe Arami (Central Swiss Alps). The American Geophysical Union, Geophysical Monograph 95, 307–329.

Gresse, P.G., Chemale Jr, F., Silva, L.C., Walraven, F., Hartmann, L.A., 1996. Late- to post-orogenic basins of the Pan-African-Brasiliano collision orogen in southern Africa and southern Brazil. Basin Research 8, 157–171.

Groves, D.I., Barley, M.E., Barnicoat, A.C., Cassidy, K.F., Fare, R.J., Hagemann, S.G., Ho, S.E., Hronsky, J.M.A., Mikucki, E.J., Mueller, A.G., McNaughton, N.J., Perring, C.S., Ridley, J.R., Vearcombe, J.R., 1992. Sub-greenschist to granulite-hosted Archaean lode-gold deposits of Yilgarn Craton: A depositional continuum from deep-sourced hydrothermal fluids in crustal scale plumbing systems. In: Glover, J.E., Ho, S.E. (Eds.), The Archaen: Terrains, Processes and Metallogeny, vol. 22. University of Western Australia Publication, Perth, Australia, pp. 325–337.

Groves, D.I., Goldfarb, R.J., Gebre-Mariam, M., Hagemann, S.G., Robert, F., 1998. Orogenic gold deposits: A proposed classification in the context of their crustal distribution and relationship to other gold deposit types. Ore Geology Reviews 13, 7–27.

Hartmann, L.A., Takehara, L., Leite, J.A.D., McNaughton, N.J., Vasconcellos, M.A.Z., 1997. Fracture sealing in zircon as evaluated by electron microprobe analyses and back-scattered electron imaging. Chemical Geology 141, 67–72.

Hasui, Y., Carneiro, C.D.R., Coimbra, A.M., 1975. The Ribeira Folded Belt. Revista Brasileira de Geociéncias 5 (4), 257–266.

Jost, H., Hartmann, L.A., 1984. Província Mantiqueira-Setor Meridional. In: Almeida, F.F.M., Hasui, Y. (Eds.), O Pré-Cambriano do Brasil. Edgard Blücher, São Paulo, Brazil, pp. 345–367.

Koppe, J.C. 1990. Metalogênese do Ouro da Mina da Bossoroca, São Sepé, RS. Universidade Federal do Rio Grande do Sul, Porto Alegre, Brazil. Unpublished PhD Thesis, 289 pp.

Koppe, J.C., Hartmann, L.A., 1988. Geochemistry of Bossoroca Greenstone Belt, southernmost Brazil. Geochimica Brasiliense 2 (2), 167–174.

Machado, N., Koppe, J.C., Hartmann, L.A., 1990. A late Proterozoic U-Pb age for the Bossoroca Belt, Rio Grande do Sul, Brasil. Journal of South American Earth Sciences 3 (2/3), 87–90.

McNaughton, N.J., Bickle, M.J., 1987. K-feldspar Pb–Pb isotope systematics of post-kinematic granitoid intrusions of the Diemals area, central Yilgarn Block, Western Australia. Chemical Geology 66, 193–208.

Remus, M.V.D. 1990. Geologia e geoquímica do Complexo Cambaizinho, São Gabriel-RS. Universidade Federal do Rio Grande do Sul, Porto Alegre, Brazil. Unpublished MSc Thesis, 267 pp.

Remus, M.V.D., Hartmann, L.A., Formoso, M.L.L., 1993. Os padrões de Elementos Terras Raras (ETR) e a afinidade geoquímica komatiítica dos xistos magnesianos e rochas associadas do Complexo Cambaizinho, São Gabriel-RS. Revista Brasileira de Geociências 23 (4), 370–387.

Remus, M.V.D., McNaughton, N.J., Hartmann, L.A., Fletcher, I.R., 1997. Zircon SHRIMP U/Pb dating and Nd isotope data of granitoids of the São Gabriel Block, southern Brazil: evidence for an Archaean/Paleoproterozoic basement. In: International Symposium on Granites and Associated Mineralizations, 2, Salvador, Brazil, Extended Abstracts, pp. 271–272.

Sartori, P.L., Rüegg, N.R., 1979. O complexo Granítico de São Sepé, Rio Grande do Sul e a evolução das rochas graníticas da região orogênica do Sudeste. Boletim do Instituto de Geociências da Universidade de São Paulo 10, 69–78.

Smith, J.B., Barley, M.E., Groves, D.I., Krapez, B., McNaughton, N.J., Bickle, M.J., Chapman, H.J., 1998. The Scholl Shear Zone, West Pilbara; evidence for a domain boundary structure from the integrated tectonostratigraphic analyses, SHRIMP U-Pb dating and isotopic and geochemical data of granitoids. Precambrian Research 88, 143–171.

Soliani Jr, E. 1986. Os dados geocronológicos do Escudo Sul-Riograndense e suas implicações de ordem geotectônica. Universidade de São Paulo, São Paulo, Brazil. Unpublished PhD Thesis, 239 pp.

Stacey, J.S., Kramers, J.D., 1975. Approximation of terrestrial lead isotope evolution by a two stage model. Earth and Planetary Science Letters 26, 207–221.

Wildner, W. 1990. Caracterização geológica e geoquímica das seqüências ultramáficas e vulcano-sedimentares da região da Bossoroca-RS. Universidade Federal do Rio Grande do Sul, Porto Alegre, Brazil. Unpublished MSc Thesis, 170 pp.

Zarpelon, P.R. 1986. Geologia estrutural, estratigrafia e petrologia de uma parte do "greenstone-belt" Cerrito do Ouro, município de São Sepé-RS Universidade Federal do Rio Grande do Sul, Porto Alegre, Brazil. Unpublished MSc Thesis, 215 pp.